Journal of Alloys and Compounds, 194 (1993) 199–211
JALCOM 7220

Diffusional aspects of the solid state amorphization reaction

A. L. Greer
University of Cambridge, Department of Materials Science and Metallurgy, Pembroke Street, Cambridge CB2 3QZ (UK)

N. Karpe and J. Bøttiger
Institute of Physics and Astronomy, University of Aarhus, DK-8000 Aarhus C (Denmark)

(Received February 2, 1992; in final form June 29, 1992)

Abstract

Diffusional aspects of the solid state amorphization reaction (SSAR), specifically in early transition metal–late transition metal (ETM–LTM) systems, are considered. Self- and tracer diffusivities of ETM and LTM components in crystalline and amorphous phases are reviewed. The alloy characteristics leading to fast diffusion of LTM species and to good glass-forming ability are described. The nucleation of the amorphous phase in the SSAR is analysed, drawing parallels with interstitial–substitutional diffusion in semiconductors. Interdiffusion in amorphous ETM–LTM phases is considered in detail, taking into account stress effects, structural relaxation and the mixing thermodynamics of the amorphous phase.

1. Introduction

There are a number of examples of interfacial reactions which can yield an amorphous phase, *e.g.* oxidation and silicidation [1]. A reaction between two polycrystalline metallic elements yielding an amorphous phase was first demonstrated by Schwarz and Johnson [2]. There are many other methods of amorphizing alloys in the solid state (reviewed in ref. 3), *e.g.* ion [4], electron [5] and neutron [6] irradiation, ion mixing [7], ion implantation [8], mechanical alloying [9], grinding of intermetallic compounds [10] and hydrogenation [11], typically involving an input of energy or a composition change. However, amorphization by interfacial reaction occurs as a system of constant average composition evolves towards equilibrium on annealing, and is the method most amenable to quantitative analysis. It is the subject of this paper, in which it is referred to as the solid state amorphization reaction (SSAR).

The SSAR is found for a large number of combinations of metals (reviewed in ref. 3), but the most common type of combination (and the most studied) is that of a late transition metal (LTM – Co, Fe, Ni) with an early transition metal (ETM – Hf, Ti, Zr). This paper focuses on the SSAR in the Fe–Zr, Co–Zr and Ni–Zr systems.

It was recognized from the earliest studies [2] that there are two main attributes of systems showing the SSAR: a strong thermodynamic driving force for the mixing of the two elements (*i.e.* a strongly negative heat of mixing) and diffusional asymmetry (*i.e.* one element diffuses anomalously fast in the other, but not vice versa). As Johnson [3] has pointed out in his review of the various methods of solid state amorphization, the transformations to form a metastable amorphous phase involve competing processes. In the SSAR the role of the diffusional asymmetry is roughly that the fast-diffusing component permits the mixing of the two elements, whereas the other relatively immobile component hinders the structural changes that would enable the system to maintain equilibrium structures appropriate for its composition. This paper is concerned with the diffusional (*i.e.* kinetic) aspects of the SSAR, which are significantly influenced by the thermodynamics of the systems involved.

2. Diffusional asymmetry

The diffusional asymmetry referred to above was noted in the crystalline forms of the two elements involved, and could form a basis for the selection of systems for the SSAR. For example, nickel is a fast diffuser in crystalline zirconium (α phase, hexagonal close packed (h.c.p.)), but zirconium has a normal (slow, substitutional) diffusivity in crystalline nickel (cubic close packed (c.c.p.)) [12]. Data on tracer and self-diffusivities in bulk and grain boundaries are collected in Fig.1 for a number of LTM–Zr combinations. Zirconium, like the other ETMs hafnium and titanium, exhibits two

0925-8388/93/$6.00

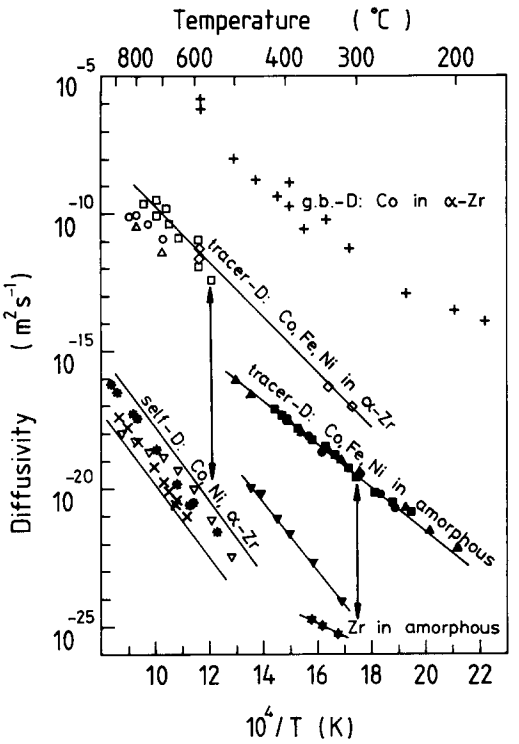

Fig. 1. Survey of data on self-diffusivities and tracer diffusivities of components of late transition metal–zirconium (LTM–Zr) systems: self-diffusivities in α-Zr (▽, [13]), c.c.p. Co (×, [14]) and Ni (*, [15]); tracer diffusivities of Co (□, in single crystal [16]; ◇, in polycrystal [17]), Fe (△, in single crystal [12]) and Ni (○, in single crystal [12]) in α-Zr; grain boundary diffusivity (times segregation factor) of Co in α-Zr (+, [17, 18]); tracer diffusivities of LTM in amorphous LTM–Zr alloys (with $x_{LTM} \geqslant 0.5$) – Co in a-$Co_{89}Zr_{11}$ (■, [19]), Fe in a-$Fe_{91}Zr_9$ (▲, [20] and Ni in a-$Ni_{50}Zr_{50}$ (●, [21]); Zr in amorphous LTM–Zr alloys (with $x_{LTM} \geqslant 0.5$) – in a-$Fe_{91}Zr_9$ (▼, [20]) and in a-$Ni_{65}Zr_{35}$ (★, [22]). The vertical arrows indicate the disparity between LTM and Zr diffusivities in α-Zr and a-LTM–Zr alloys.

crystalline phases: α at lower temperature (less than 1135 K [23]) is h.c.p.: β at higher temperature is body-centred cubic (b.c.c.). Here, only diffusivities at lower temperatures (below the α–β transition) are considered, as these are the temperatures relevant for the SSAR (and in the SSAR it is the α phase which reacts with the LTM). Some of the scatter in the data for the α phase can be attributed to anisotropy of diffusion in single-crystal or textured polycrystalline samples. From the figure it is clear that the diffusivities of LTM solutes (Co, Ni and Fe) in an α-Zr matrix are very similar and anomalously fast, being 10^6–10^9 times faster than the self-diffusivities of the elements involved (which are similar to each other). Grain boundary diffusivities for LTM solutes in α-Zr grain boundaries appear to be even higher (by 10^4–10^5 times). For both bulk and grain boundary diffusion there is a variety of evidence, including low activation volume, indicating that the anomalously fast transport is interstitial [24, 25]. Similar results are found for LTM solutes in hafnium and titanium.

The diffusional asymmetry evident in the crystalline elements also appears to be present in the amorphous phases formed by the SSAR. The diffusion in the amorphous phase is directly related to the mechanism of the SSAR since the amorphous phase forms as a barrier layer between the two reacting elements. Relevant data on tracer diffusivities of the components in a-LTM–Zr ("a" denotes amorphous) phases are included in Fig. 1. Diffusivities in a-Ni–Zr appear to be relatively independent of composition for mole fractions $x_{Ni} \geqslant 0.5$ [21], and for valid comparisons only amorphous phases with LTM mole fractions of 0.5 or greater are considered in the figure. With this restriction, the self-diffusivities of the LTM components in a-LTM–Zr phases are found to be remarkably similar (as pointed out by Dörner and Mehrer [19]). An inert marker experiment in the amorphous phase during the SSAR in the Ni–Zr system has shown that nickel is the dominant diffusing species [26]. This supports the observation for Ni–Zr [27, 28] (and more recently for Co–Zr [19]) that the rate of thickening of the amorphous layer in the SSAR is consistent with the diffusivity of nickel (or cobalt) as measured by radiotracer experiments in the amorphous phase. Within the resolution of the marker experiment, it could be concluded that the diffusivity of nickel is at least 20 times that of zirconium. In radiotracer measurements by Horváth *et al.* [20] on a-$Fe_{91}Zr_9$ it was found that the disparity between LTM and ETM diffusivities in an amorphous ETM–LTM phase could be as great as that between the LTM and ETM diffusivities in a crystalline, α phase ETM. These measurements are included in Fig. 1, and show that the LTM component can also be an anomalously fast diffuser in the amorphous alloy, being up to 10^5 times faster than the ETM component. (The disparity in LTM and ETM diffusivities is, however, much less marked in the Zr-rich amorphous phases $Fe_{24}Zr_{76}$ and $Fe_{28}Zr_{72}$ [20].) The $Fe_{91}Zr_9$ composition in which the diffusivities were measured is well outside the approximately equiatomic composition range formed by the SSAR. The first confirmation that, in the composition range of the amorphous phase formed in the SSAR, the disparity between the LTM and ETM diffusivities could be so great came in the work of Greer *et al.* [22] on multilayered thin films. They showed that in a-$Ni_{65}Zr_{35}$ the zirconium self-diffusivity is approximately 10^6 times less than that of nickel.

It appears from Fig. 1 that, in general, LTM diffusivities in a-LTM–Zr phases (with $x_{LTM} \geqslant 0.5$) are approximately 10^2 times lower than in α-Zr. Zirconium diffusivities in a-LTM–Zr phases are 10^0–10^2 times greater than the self-diffusivity in α-Zr. In a-LTM–Zr phases, and presumably in a-LTM–ETM phases more

generally, this still leaves the self-diffusivity of the LTM component much higher, by 10^3–10^6 times, than that of the ETM component. Further data and comparison may be found in the review by Dörner and Mehrer [19].

Tracer diffusivities have now been determined for several species in a-Ni–Zr. A comparison for 573 K is shown in Fig. 2. This shows clearly a tendency for smaller species to diffuse faster, with the greatest disparity being between the ETM and LTM species which occur at opposite ends of the size range. The size dependence of diffusivity can loosely be understood within the free volume model for atomic transport in liquids and glasses [32], if it is assumed that the critical free volume fluctuation for a diffusive jump scales with the volume of the diffusing species. However, it must be emphasized that the mechanisms of atomic diffusion in amorphous alloys are not yet well understood. While there appears to be a continuous range of diffusivities, at the extremes analogies with the diffusive mechanisms in crystals may be useful. The fast LTM diffusion can be regarded as predominantly interstitial, whereas the slow ETM diffusion is predominantly substitutional.

The atomic size difference between ETM and LTM components appears to be important in giving the diffusional asymmetry essential for the SSAR. Further links between atomic size difference and amorphous phase formation are explored in the next section.

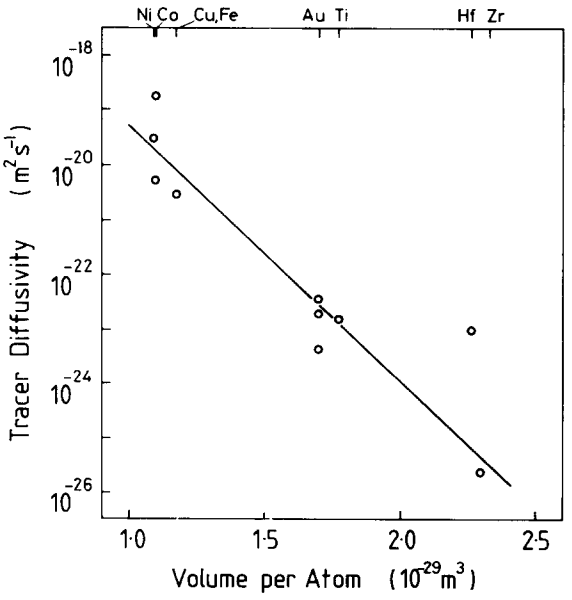

Fig. 2. Survey of data on tracer diffusivities at 573 K of various species in amorphous Ni–Zr alloys with $x_{Ni} \geq 0.5$, showing a correlation with the atomic volume of the diffusing species: Ni [21], Co [21, 29], Cu [21], Fe [21], Au [21, 30, 31], Ti [21], Hf [29] and Zr–Hf interdiffusivity [22].

3. Glass-forming ability of binary alloys

Anomalous fast diffusion of the type discussed above for LTM solutes in ETM hosts is known in several crystalline solid solutions. In each case, the host is an electropositive element with a large lattice parameter and the solute a noble metal or transition metal with filled or nearly filled d bands. The fast transport is mainly interstitial, even though in all cases the ratio of the atomic radius of the solute to that of the host (r_s/r_h) is substantially greater than the Hägg [33] empirical limit ($r_s/r_h = 0.59$) for interstitial solution. For example (taking Goldschmidt radii), for nickel in zirconium, r_s/r_h is 0.78. Interstitial solution and transport are possible because the repulsive interaction between the solute and host atoms is particularly weak, in comparison with the solute–solute and host–host repulsive interactions. Also, the equilibrium separation of host and solute atoms in intermetallic compounds is substantially less than the sum of the host and solute atomic radii in their elemental phases. Turnbull [34] first pointed out that these characteristics of elemental combinations favouring fast diffusion also favour glass formation. Turnbull [34] considered the types of binary alloy with good glass-forming ability in rapid liquid quenching, but his discussion of the structure and stability of the glassy alloys would apply equally to amorphous alloys more generally (formed by methods other than rapid liquid quenching). In particular, it is notable that many stable amorphous alloys have, as their predominant component, an element of the type which would be a solute in fast diffusion and, as a stabilizing solute, an element of the type which would be a host in fast diffusion. The weak repulsive interaction between unlike atoms, noted in connection with fast diffusion, is associated in the liquid alloys with a volume contraction on mixing the elements, a negative enthalpy of mixing and marked short-range ordering as the temperature is lowered – all characteristics of good glass-forming ability.

To aid in the selection of suitable alloys, there have been several attempts to find empirical correlations between glass-forming ability and readily available elemental parameters. Probably the most generally applicable correlations are with atomic sizes. It is found [35, 36] that, for a glass to be formed by rapid quenching of a liquid binary alloy, the atomic radii of the two components must differ by at least 10%. Two-parameter maps of glass-forming ability are useful for establishing correlations within a family of alloys (*e.g.* binary alloys of a particular metal). Among the most successful maps are those with atomic size ratio and the heat of mixing of the components [35]. Such a map for metal–Zr alloys is shown in Fig. 3. The correlation of glass-forming ability with atomic size difference was made more

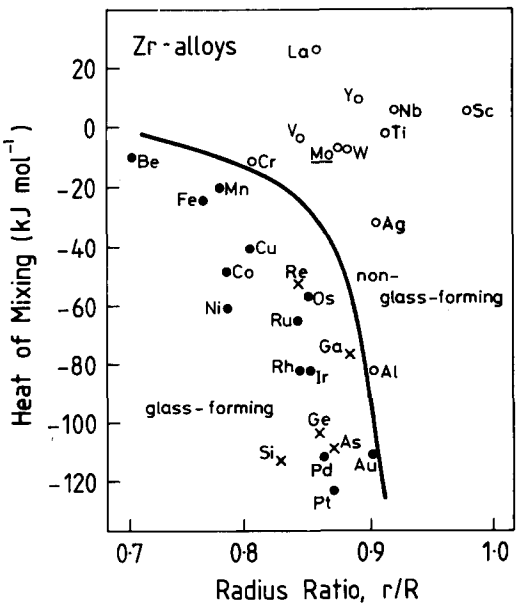

Fig. 3. A map for binary zirconium alloys showing values of the maximum heat of mixing of the components and of the atomic radius ratio (r, radius of smaller component; R, radius of larger). The filled symbols indicate that glass formation is possible by rapid liquid quenching and a distinct region of the map is seen to correspond to glass formation. Systems not yet tested are indicated by ×. (After Giessen [35].)

quantitative by Egami and Waseda [37]. They have shown that atomic size difference can be used to predict the glass-forming composition range in binary systems, the product of the minimum solute concentration for glass formation (at liquid quenching rates of approximately 10^6 K s^{-1}) and the fractional difference in atomic volume being approximately 0.1.

In conclusion, the atomic size difference found in systems such as Ni–Zr is favourable not only for the fast diffusion of nickel, but also for the stability of an amorphous phase formed by whatever means. Although tabulated values of atomic radii can be useful, the chemical considerations of Turnbull [34] show that the effective size can be modified by alloying effects and that sizes are not uncorrelated with other parameters.

4. Interstitial transport and the nucleation of the amorphous phase

When a multilayer of two polycrystalline metals is deposited for the SSAR, it is often the case that there is initially, before any annealing, a thin amorphous layer at each interface. The extent of this layer can be a sensitive probe of the deposition conditions [38, 39]. When it is present, there is no nucleation stage for the SSAR. Even for ETM–LTM combinations, however, it is possible for the interfaces in an as-deposited multilayer to be ordered, in which case there is a nucleation barrier for the SSAR [40]. The nature of this nucleation barrier was studied in Ni–Zr by Vredenberg *et al.* [41], who showed that the SSAR does not occur at the interface between polycrystalline nickel and single-crystalline zirconium. The reaction can be initiated (and once initiated will proceed into the single-crystalline zirconium) by generating a thin amorphous layer by ion mixing, or by depositing an intermediate layer of polycrystalline zirconium. Pampus *et al.* [42] showed that the SSAR in Ni–Zr does occur at an interface between polycrystalline zirconium and single-crystalline nickel. The absence of the SSAR for single-crystalline zirconium was confirmed by Ehrhart *et al.* [43] who showed, however, that there was easy nickel transport through the single-crystalline zirconium sufficient to permit nickel segregation to the other side (in contact with a niobium substrate) of the 50 nm thick zirconium. Thus it seems that, in the absence of an initial amorphous phase, zirconium grain boundaries are necessary for its nucleation. Furthermore, it seems that high-angle boundaries are necessary, as Meng *et al.* [44] have shown that low-angle grain boundaries are not effective nucleation sites.

This nucleation behaviour can be better understood by considering the interdiffusion which is likely to occur at an interface between (taking the same system) crystalline nickel and zirconium. A typical temperature for the SSAR is 573 K [40, 45], at which an amorphous layer if nucleated grows to a limiting thickness of approximately 100 nm before the crystalline intermetallic phase NiZr appears [44]. The amorphous layer would grow to 50 nm, half its limiting thickness, in approximately 2000 s [40, 45]. We now estimate diffusional penetration distances into the crystalline phases in the same time, if the amorphous phase does not nucleate. These distances are not accurately calculable because the relevant diffusivities have to be extrapolated from higher temperature data. Tracer diffusivities measured for nickel into α-Zr are, as described above, for interstitial transport and indicate in the same time a penetration distance of 0.2 μm [12]. The substitutional diffusivity of nickel in α-Zr is not known, but can be assumed to be of the same order of magnitude as the self-diffusivity of zirconium, but somewhat greater. Similarly the substitutional diffusivity of zirconium into nickel can be assumed to be similar to, but somewhat lower than, the self-diffusivity of nickel. Taking the estimated values of the self-diffusivities at 573 K [13, 15], the penetration distances in 2000 s are calculated to be 2×10^{-14} m or more for nickel into α-Zr and 1.3×10^{-13} m or less for zirconium into nickel, distances much less than an atomic monolayer. In practice, the diffusivities might not be so low as the extrapolations suggest because of vacancy supersaturation; however, it is clear that there is negligible substitutional inter-

diffusion during anneals suitable for the SSAR, and indeed negligible mixing of any kind, for although the nickel can penetrate the zirconium significantly by interstitial diffusion, the interstitial solubility is very small. Thermodynamic calculations [46] for the Ni–Zr system show that, in an equilibrium between the elemental phases, there would be considerable solid solubility on each side, but it is important to note that the calculations are for mixing in a given crystal structure, *i.e.* they assume substitutional solution. Ehrhart *et al.* [43] found that the interstitial solubility was too low to be detected. A likely solubility limit is 0.1–0.2 at.%, based on similar systems [34]. It is known, however, that interstitial solubilities can be forced to higher, non-equilibrium levels by, for example, rapid liquid quenching [47]. For copper in yttrium ($r_s/r_h = 0.71$), an interstitial solubility of up to 12.5 at.% has been reached [47].

The distinction between substitutional and interstitial solubility has, for some time, been recognized as important for diffusion in semiconductors. For example, copper diffuses interstitially in germanium, but has a small interstitial solubility. If copper diffuses into a sample of germanium, a substitutional solution is formed at all free surfaces and dislocations (and presumably also grain boundaries, if present), even those not in direct contact with the source of copper. Although the concentration of copper throughout the germanium is very low, the copper can readily be transported anywhere, and the substitutional solution forms where there is a source of vacancies on the germanium lattice, permitting the copper to move from interstitial to substitutional sites. This "interstitial–substitutional" model of Frank and Turnbull [48] can be applied to LTM solutes in ETM hosts.

In particular, we can examine the role of zirconium grain boundaries in nucleating the amorphous phase in Ni–Zr couples. At a grain boundary, the formation of an amorphous phase is analogous to the formation of a solid solution in the Frank–Turnbull model and can be understood as a type of substitutional dissolution. The amorphous phase is formed because, if the nickel segregation to a zirconium grain boundary is at all significant, the composition at the boundary would be such that a-Ni–Zr would have a lower free energy than a substitutional solution of nickel in zirconium [46]. In the same way as for copper in germanium, the grain boundary is a source of vacancies or more generally a site where the zirconium mobility is higher. It is interesting that amorphization did not occur at the semicoherent interface between zirconium and niobium in the experiment of Ehrhart *et al.* [43]. Interstitial transport through 50 nm of zirconium permitted a saturation level of two or three monolayers of nickel to adsorb on the interface, but presumably the interfacial dislocations cannot climb away from the interface to generate vacancies. Also of interest is that, as the experiments [41, 43] on single-crystalline zirconium show, the Zr–Ni interface does not itself give amorphization. In any slight substitutional interdiffusion, however, the net flow of vacancies would be into the nickel and this could stifle rearrangements in the zirconium at the interface. The easy propagation of the amorphization once started shows the rearrangement of the zirconium atoms is possible at the interface between the amorphous phase and the crystalline zirconium. The growth of the amorphous phase is considered in more detail in the next section.

5. Diffusion in the amorphous phase: relaxation effects

5.1. *Interstitial transport and composition changes*

As discussed in Section 2, it is well established that the growth rate of the amorphous phase in the SSAR is controlled by the diffusivity of the LTM component in the amorphous phase, and not by the amorphization of the relatively immobile ETM lattice at the interface with the amorphous phase. The disparity between the LTM and ETM mobilities in the amorphous phase strongly suggests that the LTM transport is interstitial in character. Yet interstitial-like transport through the amorphous layer is not the only process within the amorphous phase. As the SSAR proceeds, any point in the amorphous phase continually increases in LTM content [22]. If the changes in LTM content of the amorphous phase could be entirely accommodated by interstitial solution, there would be no need for ETM mobility. It seems more likely, however, that there is an additional process by which LTM, supplied by interstitial transport, is incorporated into the structure of the amorphous phase. This transfer of LTM from interstitial-like to substitutional-like sites is a type of structural relaxation of the amorphous phase. As non-interstitial diffusion in amorphous phases is mediated by free volume rather than by discrete vacancies, and as free volume can be created or annihilated throughout the phase (and not just at an interface) [49], the transfer of LTM from one type of site to the other can presumably occur throughout the amorphous phase. As the LTM content of the amorphous phase changes, whether incorporated interstitially or substitutionally, there are associated changes in volume. As neighbouring regions change volume differently, stresses develop. In Sections 5.2 and 5.3, we consider how diffusion in an amorphous LTM–ETM phase may be influenced by stress and by structural relaxation. The relationship of such effects to the kinetics of the SSAR has been briefly discussed previously [22].

5.2. Stress effects

Stephenson [50] has analysed thoroughly interdiffusion in binary systems with components of differing mobilities. He has shown that stresses will develop as a result of interdiffusion if the product VM, where V is the partial molal volume and M is the mobility, is different for the two components. In an amorphous solid there is no need to consider vacancy concentration or concentration gradient, and in Stephenson's treatment [50] the chemical potentials of the components are dependent only on the external conditions and on the local composition and stress state, thus excluding any possible relaxation effects (considered in Section 5.3). If the products VM differ for the two components, there is net transport by diffusion and this is assumed to be accommodated by newtonian viscous flow. Stephenson [50] shows that whether or not stresses have a significant effect on interdiffusion depends on the viscosity and the distance scale of the composition or stress profile. When regions changing volume differently are far apart, or where the viscosity is low, they exert little influence on each other; in this case the net interdiffusive mobility $\tilde{M}$ is given by the Darken [51] relation

$$\tilde{M} = x_2 M_1 + x_1 M_2 \tag{1}$$

where x_i are the average mole fractions of the two components. For systems (like LTM–ETM amorphous phases) in which the mobilities M_1 and M_2 differ greatly, $\tilde{M}$ is clearly dominated by the more mobile component. In contrast, when composition gradients are steep and viscosity is high, interdiffusion may be limited by the mobility of the slower component; this is the Nernst–Planck [52] regime in which

$$\tilde{M} = \frac{M_1 M_2}{(V_1^2 x_1 M_1 + V_2^2 x_2 M_2)\rho^2} \tag{2}$$

where ρ is the density (mol m^{-3}) of the average composition. Between these two limits there is a regime in which the rate-limiting step for interdiffusion is viscous flow. The variation of $\tilde{M}$ as a function of the wavenumber k $(=2\pi/\lambda)$ of the composition profile reduces when $M_1 \gg M_2$ to

$$\tilde{M} = \frac{\left(\frac{3\rho}{4\eta}\right)(x_2 M_1) + M_1 M_2 k^2}{\left(\frac{3\rho}{4\eta}\right) + \rho^2 x_1 V_1^2 M_1 k^2} \tag{3}$$

where η is the shear viscosity at the average composition. The interdiffusivity is related to $\tilde{M}$ by

$$\tilde{D} = \tilde{M} R T \Phi \tag{4}$$

where R is the gas constant, T is the absolute temperature and Φ is a thermodynamic factor discussed in Section 6. The form of variation of $\tilde{D}$ with λ, derived from eqns. (3) and (4), is shown in Fig. 4, which has been calculated for a-$Ni_{55}Zr_{45}$ at 529 K in order to be applicable to the interpretation of the $\tilde{D}$ measurements of Atzmon and Spaepen [53], discussed below. The mobilities M_1 and M_2 are related to the tracer diffusivities D_1^* and D_2^* by

$$M_i = \frac{D_i^*}{RT} \tag{5}$$

The tracer diffusivities at 529 K were estimated from data quoted in ref. 22 for similar compositions and temperatures to be $D_1^* \equiv D_{Ni}^* = 2.6 \times 10^{-21}$ m^2 s^{-1} and $D_2^* \equiv D_{Zr}^* = 3.3 \times 10^{-27}$ m^2 s^{-1}. The partial molal volume $V_1 \equiv V_{Ni} = 5.9 \times 10^{-6}$ m^3 mol^{-1} and the density $\rho = 1.04 \times 10^5$ mol m^{-3} at $x_1 \equiv x_{Ni} = 0.55$ were calculated from data in ref. 54. The thermodynamic factor is taken to be $\Phi = 24$, the value estimated (Section 6) for a-$Ni_{50}Zr_{50}$ at 550 K. The viscosity of a-Ni–Zr has not been measured. We assume that it is governed by the diffusivity of the slow component, through the Stokes–Einstein relation

$$\eta = \frac{k_B T}{6\pi r D_{Zr}^*} \tag{6}$$

where k_B is the Boltzmann constant and r is a characteristic radius taken to be the ionic radius [55] of

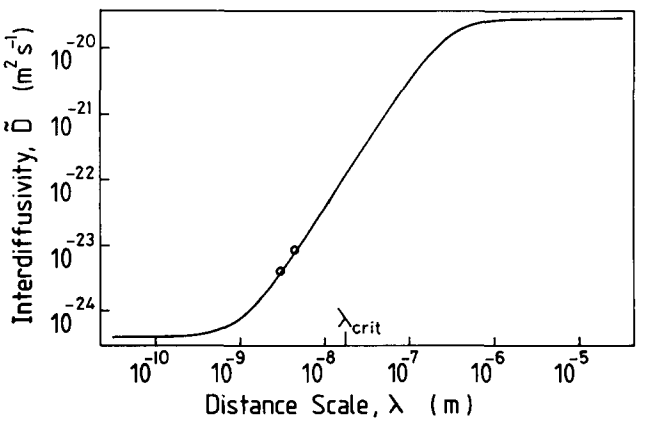

Fig. 4. Ni–Zr interdiffusivity $\tilde{D}$ in amorphous $Ni_{55}Zr_{45}$ at 529 K as a function of the distance scale of the composition or stress profile. The full line was calculated from the tracer diffusivities of Ni and Zr in the amorphous alloy using the analysis of Stephenson [50]. At large distance scale, $\tilde{D}$ is limited by the diffusion of the faster component (the Darken regime); at small distance scale, $\tilde{D}$ is limited by the diffusion of the slower component (the Nernst–Planck regime); between these regimes $\tilde{D}$ is controlled by the rate of plastic deformation. For a-$Ni_{55}Zr_{45}$ the transition in behaviour occurs at $\lambda_{crit} = 17$ nm. The data points are interdiffusivities measured in amorphous compositionally modulated multilayers of average composition $Ni_{55}Zr_{45}$ by Atzmon and Spaepen [53].

zirconium. Our estimate of η (529 K) is 1.25×10^{15} Pa s. The critical distance scale λ_{crit} for the composition profile marking the middle of the transition from Darken to Nernst–Planck behaviour is given by [50]

$$\lambda_{crit}=2\pi\left(\frac{16\eta^2 x_1 M_1 M_2 V_1^2}{9x_2}\right)^{1/4} \quad (7)$$

and for a-$Ni_{55}Zr_{45}$ at 529 K is estimated to be 17 nm. Interdiffusion when the composition profiles have distance scales of this order or smaller is expected to be dominated by stress effects.

The measurements of Atzmon and Spaepen [53] were on compositionally modulated amorphous thin films and showed that $\tilde{D}$ was dependent on the wavelength (~3 nm $<\lambda<\sim5$ nm) of the (approximately sinusoidal) composition modulation. For $\lambda=3$ nm and 4.5 nm, $\tilde{D}$ was found to be 4.0×10^{-24} m^2 s^{-1} and 8.45×10^{-24} m^2 s^{-1} respectively. These values are in contrast with the interdiffusivity estimated in the Darken regime (stress insignificant, eqns. (1), (4) and (5)), given by $\tilde{D}=2.81\times10^{-20}$ m^2 s^{-1} at 529 K. That the interdiffusivity measured by Atzmon and Spaepen [53] is three to four orders of magnitude less than the value expected in the Darken regime shows clearly that there is a strong limitation on interdiffusion, presumably stress, consistent with the Stephenson analysis [50] and our estimate of λ_{crit}. Furthermore, the measured values of $\tilde{D}$ at $\lambda=3$ nm and 4.5 nm are found to lie very close to the calculated line in Fig. 4. While this lends strong support to the suggested interpretation, such close agreement must be regarded as largely fortuitous, given the uncertainties in the material parameters (notably viscosity) and in the application of such a large thermodynamic factor as $\Phi=24$ within the Darken analysis (Section 6 [56]). Furthermore, with the step concentration gradients at which stress effects are important, there may also be chemical gradient–energy effects on the interdiffusion [53].

5.3. *Structural relaxation effects*

In a typical SSAR experiment, diffusion distances are somewhat greater than the critical wavelength estimated for a-Ni–Zr, and therefore stress effects are not expected to dominate. However, slow structural relaxation can still inhibit interdiffusion, particularly when (unlike the previous case) the average composition of the amorphous phase is changing. Evidence for relaxation effects was reported in our earlier results [22, 57, 58] on trilayered thin films consisting of a 40–45 nm thick amorphous LTM–Zr layer (LTM ≡ Co, Ni or Fe) sandwiched between two elemental layers of LTM. The in-diffusion of mobile LTM atoms into the amorphous layer is analogous to that occurring during the SSAR and causes significant composition changes; it must be analysed as chemical diffusion, not self- or tracer diffusion. It is important to take into account the changes in the Gibbs' free energy of the amorphous phase as the reaction proceeds. In principle, the composition of the amorphous phase should change until metastable equilibrium is achieved. The original aim of the experiments was to determine the metastable equilibrium (common tangent) composition of the amorphous phase in contact with the LTM elemental layer during solid state amorphization. However, as indicated by our data (reviewed below), the diffusional asymmetry between zirconium and the very mobile LTM elements (Section 2) means that the metastable equilibrium composition cannot readily be achieved.

As the LTM elements diffuse into the LTM–Zr amorphous alloy, the relative inability of the zirconium atoms to move impedes the evolution of local atomic configurations which would be necessary to maintain the amorphous phase in internal equilibrium. As described in Section 5.1, this may be thought of as the LTM atoms moving from interstitial to substitutional sites. The loss of internal equilibrium implies that, during composition changes due to LTM in-diffusion into an amorphous layer, the Gibbs' free energy of the amorphous phase will evolve along a path of higher values than those for the fully relaxed case. This hypothetical effect is illustrated in Fig. 5. The two broken lines correspond to different starting compositions for

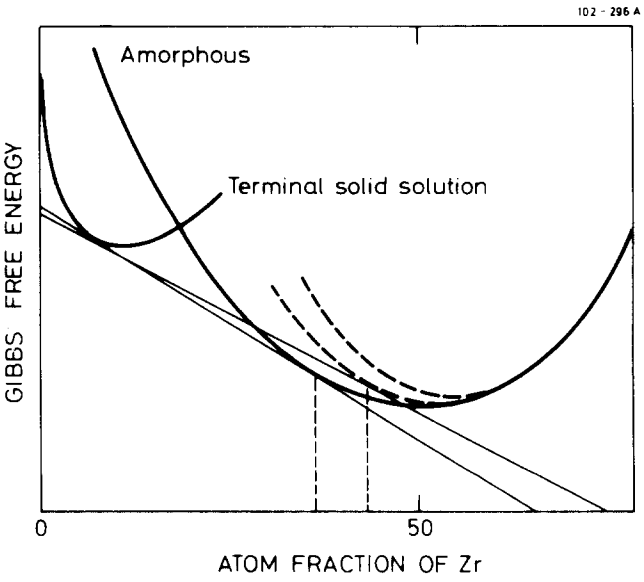

Fig. 5. A schematic Gibbs' free energy diagram for the Co–Zr (or Ni–Zr) system, showing the curve for the crystalline solid solution of cobalt (or nickel) and the curve (full line) for the amorphous phase in internal equilibrium. If the amorphous phase changes its composition, it is difficult for it to remain in internal equilibrium and its actual free energy (broken lines) may be higher, giving a changed metastable equilibrium composition (from the common tangent constructions shown) in contact with the elemental solid solution.

the amorphous phase. It is important to note that this effect of the diffusional asymmetry would imply different compositions for the metastable equilibria, as illustrated in Fig. 5 by the common tangents for the crystalline solid solution and the amorphous phase. Stresses developing as a result of composition change in the amorphous layer will have effects which, although expected to be small, could also be described by Fig. 5. In the following, "relaxation" is used to mean either structural or stress relaxation, but structural relaxation is presumed to be dominant.

In Fig. 6, the results of annealing experiments in trilayered Co–$Co_{100-x}Zr_x$–Co films are summarized [22, 57, 58]. The changes in the composition at the middle of the amorphous middle layer, which were measured using Rutherford backscattering spectroscopy (RBS), are shown. The results from both sputter-deposited and electron-beam-evaporated films are included in the figure. For both types of films a similar in-diffusion of cobalt on annealing is observed. In Fig. 6 the arrows denote irradiation with 1×10^{15} Xe^+ ions cm^{-2} at 500 keV between anneals. The broken lines show the behaviour on annealing following irradiation. Transport of ions in matter (TRIM) [59] calculations with a displacement threshold energy of 25 eV suggest that this dose corresponds to an average of approximately 17 displacements per atom (d.p.a.) in the middle layer. Although this is sufficient to displace essentially all the atoms, it is not enough to cause significant long-range atomic mixing, as discussed elsewhere [60]. Furthermore, no difference was observed in the in-diffusion rate between films which had been irradiated prior to the first anneal and unirradiated films of the same composition.

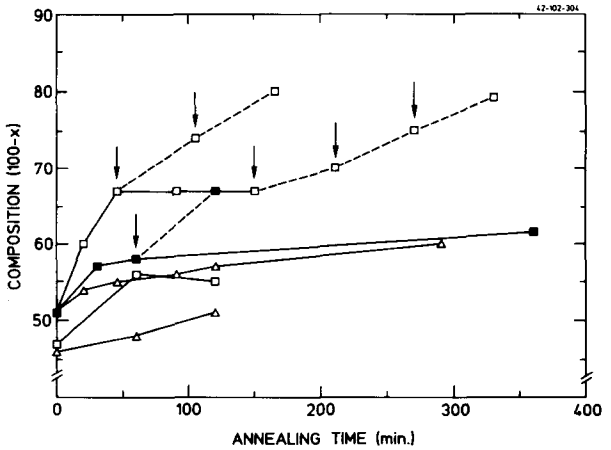

Fig. 6. The composition of the midpoint of the amorphous layer in trilayer Co–$Co_{100-x}Zr_x$–Co films after chemical diffusion of cobalt from the outer elemental crystalline layers during annealing at 693 K (□), 673 K (■) and 653 K (△). The arrows and the corresponding broken lines denote irradiation with 1×10^{15} Xe^+ cm^{-2} at 500 keV at room temperature prior to annealing. (After ref. 58.)

Without irradiation, the in-diffusion is found to level off at different compositions, depending on temperature. Although the composition of the relaxed amorphous phase in metastable equilibrium with the elemental cobalt layer is, in principle, temperature dependent, the composition could not show a strong temperature dependence. Also, particularly at the lower annealing temperatures, there is still a slow upward drift of the cobalt content after the initial rapid rise. Thus it is clear that the metastable equilibrium with the relaxed amorphous phase has not been achieved in these anneals. In accordance with the model sketched in Fig. 5, the cobalt contents at which the in-diffusion levels off are higher for higher initial cobalt contents and for higher temperature. At higher temperature more relaxation of the zirconium configuration is possible. The drift in saturation cobalt content at lower temperatures may reflect an ongoing slow zirconium relaxation. A significant enhancement of the in-diffusion is observed if a sample with saturated cobalt content is irradiated before further annealing. The substrate temperature during the irradiation at room temperature (300 K) is below [60, 61] the critical temperature where radiation-enhanced diffusion sets in; thus the accelerated in-diffusion cannot occur during the irradiation. Also, as pointed out above, irradiation has no effect on the diffusion into samples not previously annealed. We suggest that the irradiation assists relaxation of the amorphous phase, which has an unrelaxed configuration because of prior in-diffusion. The irradiation may enable the relatively immobile zirconium atoms to adjust their configurations to the changed composition, in that way lowering the free energy of the amorphous phase. Consequently, the activity of the cobalt in the amorphous phase will decrease and there will be a driving force for further in-diffusion, as observed. Clearly, further studies are needed to understand better the role of heavy-ion irradiation prior to annealing, in particular to distinguish the effects of structural relaxation and stress relaxation in the amorphous phase.

As shown in Fig. 6, the Co content at the middle of the amorphous layer rises at a decreasing rate (best illustrated at lower temperature, *e.g.* 653 K, where the pseudo-saturation is reached less quickly). It has been pointed out elsewhere that this behaviour can be interpreted as being due to diffusion limitation [58]. However, it should be noted that it is not the intrinsic mobility of the cobalt that is rate limiting, but rather the relaxation effects discussed above which inhibit the diffusion. Taking the tracer diffusivity of cobalt in these samples to be the same as that measured in a-$Co_{89}Zr_{11}$ [19] (as seems reasonable, to a good approximation), the diffusion penetration depth would equal the amorphous film thickness (45 nm) after just 5 min at 653 K. In contrast, the data in Fig. 6 show diffusional

kinetics extending far beyond this time. The slower kinetics are interpreted here as reflecting primarily the difficulty of getting the cobalt into substitutional solution in the amorphous phase.

In-diffusion has also been studied in trilayer films of Ni–$Ni_{100-x}Zr_x$–Ni with $x=33$, 48, 50 and 51 at.%. The nickel content of the amorphous middle layer after annealing at 673 K is shown in Fig. 7 for films with starting compositions $x=33$ and 51 at.%. There is the same tendency as with the Co–Zr trilayers for the in-diffusion to level off before metastable equilibrium with the relaxed amorphous phase is achieved.

In Fig. 8 the composition changes in the amorphous middle layer of Fe–$Fe_{100-x}Zr_x$–Fe films are shown after 1 h anneals at 723, 773 and 823 K [62]. In Fe–$Fe_{44}Zr_{56}$–Fe, a net out-diffusion of iron from the amorphous layer is observed, while in Fe–$Fe_{53}Zr_{47}$–Fe in-diffusion is observed. For Fe–$Fe_{67}Zr_{33}$–Fe, no compositional change could be detected within our experimental resolution in RBS of approximately 1 at.%. These results are incompatible with there being a single common tangent composition which is being approached, but can be explained if the amorphous Fe–Zr phase has a Gibbs' free energy varying with composition as shown in Fig. 9. Here the free energy has two minima with a maximum at approximately 50 at.%. Thus the in-diffusion and out-diffusion measurements directly indicate a tendency to phase separation in amorphous Fe–Zr, as was originally proposed by Krebs *et al.* [63], based on indirect evidence from magnetic measurements. It should be noted that Ni–Zr and Co–Zr, showing relatively rapid in-diffusion, are well known to exhibit complete solid state amorphization [40, 64]. In contrast, the Fe–Zr system, exhibiting phase separation and very

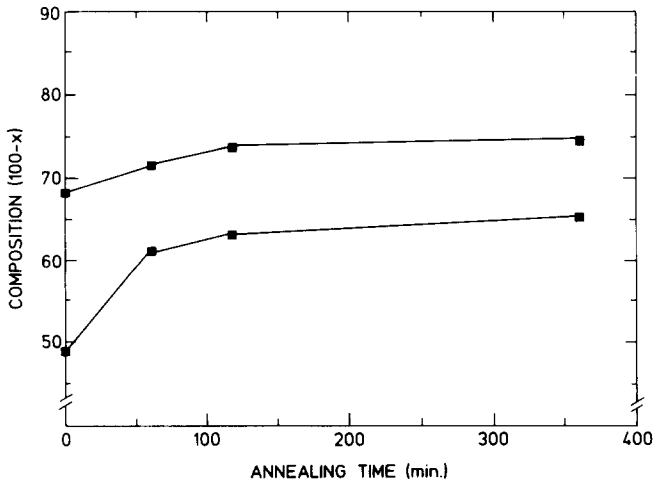

Fig. 7. The composition of the midpoint of the amorphous layer in trilayer Ni–$Ni_{100-x}Zr_x$–Ni films after chemical diffusion of nickel from the outer elemental crystalline layers during annealing at 673 K. The starting compositions of the amorphous phase are $x=33$ and $x=51$ at.%. (After ref. 58.)

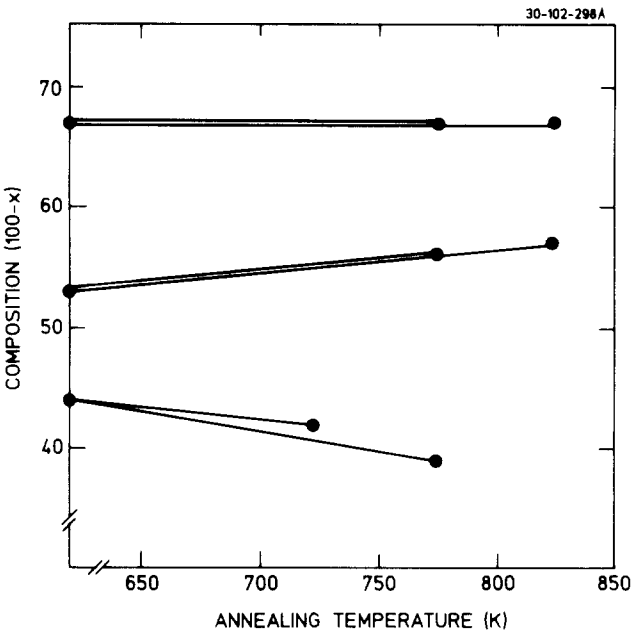

Fig. 8. The composition of the midpoint of the amorphous layer in trilayer Fe–$Fe_{100-x}Zr_x$–Fe films after chemical diffusion of iron from or to the outer elemental crystalline layers during 1 h anneals at 723, 773 and 823 K. (After ref. 58.)

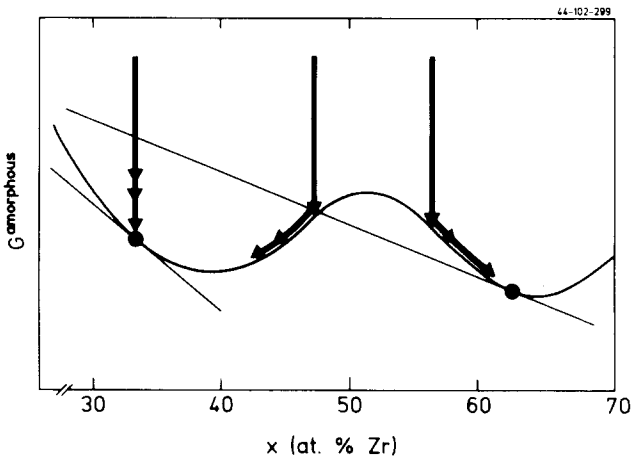

Fig. 9. Schematic Gibbs' free energy diagram for amorphous Fe–Zr, showing that phase separation is thermodynamically favourable. The arrows correspond to the composition changes observed in trilayer diffusion experiments (Fig. 8).

sluggish in-diffusion, has been found not to exhibit complete solid state amorphization [65].

In summary, our studies of trilayered thin films show that the diffusion of the LTM into amorphous films of Co–Zr, Ni–Zr and Fe–Zr is not as fast or as great as would be expected from tracer diffusivities of the LTM. It is proposed that the inhibition of the in-diffusion arises from a sluggish relaxation process, and that this process is the transfer of LTM from interstitial to substitutional sites in the amorphous phase. Stress effects are not expected to be dominant at the diffusion distances involved, but cannot be ruled out. Structural,

rather than stress, relaxation effects should be important when, as in all the trilayer experiments, the average composition of the amorphous phase is changing.

Some further evidence for sluggish relaxation processes in amorphous ETM–LTM systems comes from experiments by Tu and Chou [66] on amorphous trilayers $Ni_{40}Zr_{60}$–$Ni_{73}Zr_{27}$–$Ni_{40}Zr_{60}$. On annealing, nickel diffuses out of the central layer, and at intermediate temperatures this is accompanied by voiding, suggesting that the relatively immobile zirconium cannot readily accommodate the consequent volume change.

6. Diffusion in the amorphous phase: thermodynamic effects

In this section we review our earlier, more conventional interdiffusion measurements [58], examining the influence of the mixing thermodynamics of the amorphous phase on the rate of diffusion in the SSAR. As described in Section 2, the three elements Co, Ni and Fe have very similar atomic sizes and similar diffusion behaviour in α-Zr and in their amorphous alloys with Zr. This suggests that the sluggish in-diffusion of Fe into amorphous Fe–Zr described in Section 5.3 originates from the thermodynamic influence on chemical diffusion. To investigate this, we studied interdiffusion in composition-graded amorphous thin films of Fe–Zr and Ni–Zr. Although there may be structural or stress relaxation effects (as described in Section 5) in these measurements, the effects should be small and should in any case be very similar for Fe–Zr, so not affecting the comparison of the two systems.

The chemical diffusivity of nickel in amorphous Ni–Zr has been determined from films having the average composition of $Ni_{48}Zr_{52}$ and an initial composition graded monotonically from $Ni_{54}Zr_{46}$ to $Ni_{43}Zr_{57}$ through a thickness of approximately 120 nm [58]. The composition profile was determined by RBS to be approximately sinusoidal with a period equal to twice the film thickness. It should be noted that the distance scale of this composition profile is well in excess of the critical value, 17 nm (Section 5.2), below which stress effects should be significant. The interdiffusion coefficient was derived from an analysis of the time dependence of the composition during annealing, using a standard solution of the diffusion equation

$$c(y, t) = c(y, t=0)\exp(-k^2\tilde{D}t) \quad (8)$$

where $c(y, t)$ is the deviation from the average composition and $k = 2\pi/2d$ with d being the thickness of the film. The interdiffusivities $\tilde{D}$ of amorphous $Ni_{48}Zr_{52}$, evaluated at selected annealing temperatures from the change in composition profile measured by RBS [58], are shown in Fig. 10. Data from Hahn *et al.* [67]

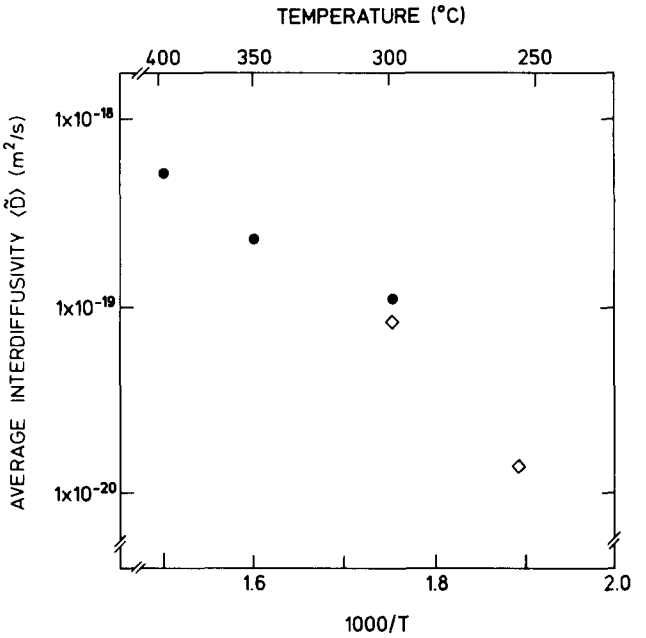

Fig. 10. Average interdiffusivity $\langle\tilde{D}\rangle$ in an amorphous thin film (120 nm thick) of average composition $Ni_{48}Zr_{52}$, with composition graded through its thickness from $Ni_{54}Zr_{46}$ to $Ni_{43}Zr_{57}$ (●). Data on $\langle\tilde{D}\rangle$ in an amorphous sample graded from $Ni_{61}Zr_{39}$ to $Ni_{33}Zr_{67}$ from ref. 67 are shown for comparison (◇).

obtained using the same method are shown for comparison. Rearranging eqns. (1), (4) and (5), we have the well-known Darken equation [51]

$$\tilde{D} = (x_2D_1^* + x_1D_2^*)\Phi = x_2D_1 + x_1D_2 \quad (9)$$

where D_i are the chemical diffusivities of the components. Because the diffusivity of Zr can be assumed to be negligible [22], the chemical diffusivity of nickel can be evaluated as $D_{Ni} = \tilde{D}/x_{Zr}$.

In identical experiments on graded amorphous films with compositions averaging in each case $Fe_{50}Zr_{50}$, but ranging between $Fe_{70}Zr_{30}$–$Fe_{30}Zr_{70}$, $Fe_{60}Zr_{40}$–$Fe_{40}Zr_{60}$ and $Fe_{55}Zr_{45}$–$Fe_{45}Zr_{55}$, no compositional changes could be detected within our experimental resolution after annealing for 6 h at 723 K or for 4 h at 823 K. After the treatment at 823 K, incipient crystallization could be detected in the Zr-rich regions of some films with a larger composition range. The lack of detectable interdiffusion enables us to establish an upper limit using eqn. (2) for the interdiffusivity in amorphous $Fe_{50}Zr_{50}$ at 723 K. Taking $D_{Fe} = \tilde{D}/x_{Fe}$, the corresponding upper limit on the average chemical diffusivity of iron D_{Fe} is 5×10^{-21} m^2 s^{-1}.

We now attempt to understand this low value in terms of the mixing thermodynamics of the amorphous Fe–Zr phase. First, however, it is important to note the difficulties with chemical diffusivity measurements in metallic glasses. One problem is that the measured diffusivity can only be an average diffusivity for the

whole of the composition range in the experiment. Of greater importance is the influence of structural relaxation in the amorphous phase [49, 68]. The relaxation, which causes a reduction in diffusivity, is more complete in higher temperature diffusion anneals. Consequently, measured activation energies for diffusion are often erroneously low and without direct physical significance. In contrast with tracer diffusion measurements, the composition range necessary in samples for chemical diffusion measurements limits the possibilities for thermal treatments. Experimentally it is very difficult to maintain a sample in the same state of relaxation during a series of measurements or to compare different samples in the same degree of relaxation.

The thermodynamic factor Φ in eqns. (4) and (9) arises from the non-ideal mixing of the components. For a given system it is a function of composition and temperature, and has the form

$$\Phi = \frac{x_1 x_2}{RT}\left(\frac{\partial^2 G}{\partial x^2}\right) \tag{10}$$

where G is the molar Gibbs' free energy of the phase in which the diffusion is occurring. Clearly the chemical diffusivity is strongly influenced by the composition dependence of G and will even be negative if $\partial^2 G/\partial x^2$ is negative. For a regular solution at the equiatomic composition, eqn. (10) reduces to

$$\Phi = 1 - \frac{2\Delta H_{\text{mix}}}{RT} \tag{11}$$

where ΔH_{mix} is the molar heat of mixing at the equiatomic composition. The tracer diffusivities of iron in a-Fe–Zr [20] and of nickel in a-Ni–Zr [67] have been measured by radiotracer techniques. Table 1 shows estimated values of tracer and chemical diffusivities of the LTM in amorphous Fe–Zr and Ni–Zr at 550 K. The ratio of the average chemical diffusivity to the tracer diffusivity $\langle D_{\text{LTM}}\rangle/D_{\text{LTM}}{}^*$ is found to be less than unity for a-$Fe_{50}Zr_{50}$ and approximately 14 in a-$Ni_{48}Zr_{52}$. This ratio is the thermodynamic factor in eqn. (3), but these diffusion measurements can only give a rough estimate of it, because of the relaxation effects mentioned earlier. The thermodynamic factor can also be estimated from the empirical analysis of Miedema and coworkers [69] (values for the equiatomic composition also in Table 1) which fails to indicate any phase separation in a-Fe–Zr (Section 3), but which does agree with experiment insofar as the thermodynamic factor for a-Ni–Zr is more positive than that for a-Fe–Zr. It may be that the regular solution model is not a good approximation for a-Fe–Zr, in which the enthalpy of mixing appears to be negative while there is a tendency for phase separation. In any case, the thermodynamic factor in a-Fe–Zr must be small within the miscibility gap, and this is consistent with the chemical diffusivity of iron being smaller than its tracer diffusivity. Further experiments are under way to clarify the relationship between the tracer and chemical diffusivities of nickel in a-Ni–Zr, as it has been suggested that the Darken relation (eqn. (9)) might break down in a system with a strongly negative heat of mixing [56], with $\tilde{D}$ not being as strongly enhanced by Φ as expected. In these experiments, care is being taken to ensure that the comparison of diffusivities is in samples with the same degree of relaxation.

TABLE 1. A comparison of tracer $D_{\text{LTM}}{}^*$ and chemical $\langle D_{\text{LTM}}\rangle$ diffusivities at average composition of the late transition metal (LTM) components in amorphous Ni–Zr and Fe–Zr alloys at 550 K. The thermodynamic factor Φ in the Darken relation (eqn. (9)) has been calculated for the equiatomic composition. This should equal the measured ratio $\langle D_{\text{LTM}}\rangle/D_{\text{LTM}}{}^*$, but experimental uncertainties are large

Parameter	$Fe_{50}Zr_{50}$	$Ni_{50}Zr_{50}$
$\langle D_{\text{LTM}}\rangle$[a] ($m^2\ s^{-1}$)	$<0.5\times10^{-20}$	10×10^{-20}
$D_{\text{LTM}}{}^*$ ($m^2\ s^{-1}$)	0.5×10^{-20}[b]	0.7×10^{-20}[c]
$\langle D_{\text{LTM}}\rangle/D_{\text{LTM}}{}^*$	<1	14
Φ[d]	13	24

[a]Values from ref. 58 for a-$Ni_{48}Zr_{52}$.
[b]Value interpolated from ref. 20.
[c]Value from ref. 27.
[d]Thermodynamic factor estimated for a regular solution using eqn. (11), with the heat of mixing at the equiatomic composition calculated from the semi-empirical model of Miedema and coworkers [69].

In summary, chemical diffusivity studies confirm the importance of the thermodynamic factor in eqn. (9). In spite of a large negative heat of mixing and a relatively large tracer diffusivity for iron, the chemical diffusivity of iron in a-Fe–Zr is low and the Fe–Zr system exhibits only a poor amorphous phase-forming tendency in the SSAR, in comparison with Ni–Zr and Co–Zr. The small chemical diffusivity in a-Fe–Zr arises from a low value of the thermodynamic factor associated with the phase's tendency to phase separation.

7. Conclusions

Diffusional aspects of the solid state amorphization reaction (SSAR) in early transition metal–late transition metal (ETM–LTM) systems have been reviewed. The LTM components are anomalous fast diffusers in crystalline ETM hosts, but not vice versa. Fast, interstitial-like transport also appears to apply to the LTM component in ETM–LTM amorphous alloys. The size difference between the LTM and ETM species and their bonding characteristics lead to this diffusional asymmetry, but are also associated with relatively stable and easily formed amorphous structures. The amorphous

phase may be present at as-deposited ETM–LTM interfaces but, if it is not, grain boundaries in the ETM elemental phase are necessary for its nucleation. The formation of the amorphous phase at ETM grain boundaries is considered to be analogous to the formation of a substitutional solid solution at semiconductor grain boundaries in the interstitial–substitutional model of Frank and Turnbull [48]. During nucleation and growth of the amorphous phase the dominant transport mechanism is interstitial, with substitutional mixing being negligible. However, compositional changes in the amorphous phase lead to the development of stresses. According to the analysis of Stephenson [50], it is estimated that stress effects will significantly inhibit interdiffusion in the amorphous phase for composition changes over distances less than approximately 17 nm, and there is quantitative evidence for this in compositionally modulated a-Ni–Zr. Composition changes also require structural relaxation of the amorphous phase which can be viewed as transfer of the LTM component from interstitial-like to substitutional-like sites. Evidence for inhibition of diffusion by sluggish relaxation kinetics is found in trilayer in-diffusion experiments on a-Co–Zr and a-Ni–Zr, which show that ion irradiation can stimulate the structural relaxation and permit further in-diffusion of the LTM component. The role of stresses in these experiments is presumed to be small, but remains to be clarified. A comparison of the diffusion of Fe in a-Fe–Zr and a-Ni–Zr shows that while the tracer diffusivities are very similar, the chemical diffusivity of iron is very low. This is related to the behaviour in trilayer experiments on a-Fe–Zr in which both in-diffusion and out-diffusion of iron were found, showing a tendency for phase separation in the amorphous phase. This leads to relatively sluggish diffusion and poor amorphization in Fe–Zr.

References

1 S. Herd, K. N. Tu and K. Y. Ahn, *Appl. Phys. Lett., 42* (1983) 597.
2 R. B. Schwarz and W. L. Johnson, *Phys. Rev. Lett., 51* (1983) 415.
3 W. L. Johnson, *Prog. Mater. Sci., 30* (1986) 81.
4 M. Nastasi, D. Lilienfeld, H. H. Johnson and J. W. Mayer, *J. Appl. Phys., 59* (1986) 4011.
5 D. E. Luzzi and M. Meshii, *J. Less-Common Met., 140* (1988) 193.
6 D. Lesueur, *Fizika, 2* (1970) 13.
7 B. X. Liu, W. L. Johnson and M.-A. Nicolet, *Appl. Phys. Lett., 42* (1983) 45.
8 G. K. Hubler, I. L. Singer and C. R. Clayton, *Mater. Sci. Eng., 19* (1985) 203.
9 C. C. Koch, O. B. Cavin, C. G. McKamey and J. O. Scarbrough, *Appl. Phys. Lett., 43* (1983) 1017.
10 R. B. Schwarz, R. R. Petrich and C. K. Saw, *J. Non-Cryst. Solids, 76* (1985) 281.
11 X. L. Yeh, K. Samwer and W. L. Johnson, *Appl. Phys. Lett., 42* (1983) 242.
12 G. M. Hood and R. J. Schultz, *Philos. Mag., 26* (1972) 329.
13 J. Horváth, F. Dyment and H. Mehrer, *J. Nucl. Mater., 126* (1984) 206.
14 W. Bussmann, Ch. Herzig, W. Rempp, K. Maier and H. Mehrer, *Phys. Status Solidi A, 56* (1979) 87.
15 K. Maier, H. Mehrer, E. Lessmann and W. Schüle, *Phys. Status Solidi, 78* (1976) 689.
16 G. V. Kidson, *Philos. Mag. A, 44* (1981) 341.
17 K. Vieregge, *Ph.D. Thesis,* University of Münster, 1990.
18 K. Vieregge and Ch. Herzig, *J. Nucl. Mater., 175* (1990) 29.
19 W. Dörner and H. Mehrer, *Phys. Rev. B, 44* (1991) 101.
20 J. Horváth, J. Ott, K. Pfahler and W. Uhlfert, *Mater. Sci. Eng., 97* (1988) 409.
21 H. Hahn, R. S. Averback and H.-M. Shyu, *J. Less-Common Met., 140* (1988) 345.
22 A. L. Greer, K. Dyrbye, L.-U. Aaen Andersen, R. E. Somekh, J. Bøttiger and J. Janting, *Mater. Res. Soc. Symp. Proc., 187* (1991) 3.
23 I. Barin, O. Knacke and O. Kubaschewski, *Thermochemical Properties of Inorganic Substances,* Springer, Berlin, 1973.
24 G. M. Hood, *J. Phys. F, 8* (1978) 1677.
25 K. Vieregge, C. Herzig and W. Lojkowski, *Scr. Metall. Mater., 25* (1991) 1707.
26 Y.-T. Cheng, W. L. Johnson and M.-A. Nicolet, *Appl. Phys. Lett., 47* (1985) 800.
27 K. Hoshino, R. S. Averback, H. Hahn and S. J. Rothman, *J. Mater. Res., 3* (1988) 55.
28 R. J. Highmore, J. E. Evetts, A. L. Greer and R. E. Somekh, *Appl. Phys. Lett., 50* (1987) 566.
29 H.-M. Wu and R. S. Averback, *Appl. Phys. Lett., 56* (1990) 2619.
30 J. Bøttiger, K. Dyrbye, K. Pampus and B. Torp, *Int. J. Rapid Solid., 2* (1986) 191.
31 D. Akhtar, B. Cantor and R. W. Cahn, *Acta Metall., 30* (1982) 1571.
32 D. Turnbull and M. H. Cohen, *J. Chem. Phys., 52* (1970) 3038.
33 G. Hägg, *Z. Phys. Chem., 8* (1930) 445.
34 D. Turnbull, *J. Phys. (Paris) Colloq., 4* (1976) 1.
35 B. C. Giessen, in T. Masumoto and K. Suzuki (eds.), *Proc. 4th Int. Conf. on Rapidly Quenched Metals,* Vol. 1, Japan Institute of Metals, Sendai, 1982, p. 213.
36 F. Sommer, M. Fripan and B. Predel, in T. Masumoto and K. Suzuki (eds.), *Proc. 4th Int. Conf. on Rapidly Quenched Metals,* Vol. 1, Japan Institute of Metals, Sendai, 1982, p. 209.
37 T. Egami and Y. Waseda, *J. Non-Cryst. Solids, 64* (1984) 113.
38 R. J. Highmore, R. E. Somekh, A. L. Greer and J. E. Evetts, *Mater. Sci. Eng., 97* (1988) 83.
39 R. J. Highmore, R. E. Somekh, J. E. Evetts and A. L. Greer, *J. Less-Common Met., 140* (1988) 353.
40 B. M. Clemens, *Phys. Rev. B, 33* (1986) 7615.
41 A. M. Vredenberg, J. F. M. Westendorp, F. W. Saris, N. M. van der Pers and Th. H. de Keijser, *J. Mater. Res., 1* (1986) 774.
42 K. Pampus, K. Samwer and J. Bøttiger, *Europhys. Lett., 3* (1987) 581.
43 P. Ehrhart, R. S. Averback, H. Hahn, S. Yadavalli and C. P. Flynn, *J. Mater. Res., 3* (1988) 1276.
44 W. J. Meng, C. W. Nieh, E. Ma, B. Fultz and W. L. Johnson, *Mater. Sci. Eng., 97* (1988) 87.
45 B. M. Clemens, W. L. Johnson and R. B. Schwarz, *J. Non-Cryst. Solids, 61, 62* (1984) 817.
46 N. Saunders and P. Miodownik, *J. Mater. Res., 1* (1986) 38.

47 B. C. Giessen, R. Ray and S. Hahn, *Phys. Rev. Lett., 26* (1971) 509.
48 C. Frank and D. Turnbull, *Phys. Rev., 104* (1956) 617.
49 A. I. Taub and F. Spaepen, *Acta Metall., 28* (1980) 1781.
50 G. B. Stephenson, *Acta Metall., 36* (1988) 2663.
51 L. S. Darken, *Trans. AIME, 175* (1948) 184.
52 A. R. Cooper, *J. Non-Cryst. Solids, 14* (1974) 65.
53 M. Atzmon and F. Spaepen, *Mater. Res. Soc. Symp. Proc., 80* (1987) 55.
54 Z. Altounian and J. O. Strom-Olsen, *Phys. Rev. B, 27* (1983) 4149.
55 L. Battezzati and A. L. Greer, *Acta Metall., 37* (1989) 1791.
56 M. Atzmon, *Phys. Rev. Lett., 65* (1990) 2889.
57 L.-U. Aaen Andersen, J. Bøttiger, J. Janting, N. Karpe, K. K. Larsen, A. L. Greer and R. E. Somekh, *Mater. Sci. Eng. A, 133* (1991) 415.
58 N. Karpe, J. Bøttiger, A. L. Greer, J. Janting and K. Kyllesbech Larsen, *J. Mater. Res., 7* (1992) 926.
59 J. P. Biersack and L. G. Haggmark, *Nucl. Instrum. Methods, 174* (1980) 257.
60 J. Bøttiger, K. Pampus and B. Torp, *Europhys. Lett., 4* (1987) 915.
61 L. E. Rehn and P. R. Okamoto, *Nucl. Instrum. Methods B, 39* (1989) 104.
62 N. Karpe, J. Bøttiger, J. Janting and K. Kyllesbech Larsen, *Philos. Mag., 63* (1991) 309.
63 H. U. Krebs, D. J. Webb and A. F. Marshall, *Phys. Rev. B, 35* (1987) 5392.
64 K. Samwer, *Phys. Rep., 161* (1988) 1.
65 B. M. Clemens and M. J. Suchoski, *Appl. Phys. Lett., 47* (1985) 943.
66 K. N. Tu and T. C. Chou, *Phys. Rev. Lett., 61* (1988) 1863.
67 H. Hahn, R. S. Averback and S. J. Rothman, *Phys. Rev. B, 33* (1986) 8825.
68 E. H. Chason and T. Mizoguchi, *Mater. Res. Soc. Symp. Proc., 80* (1987) 61.
69 R. F. de Boer, R. Boom, W. C. M. Mattens, A. R. Miedema and A. K. Niessen, *Cohesion in Metals,* North-Holland, Amsterdam, 1989.